Design and Optimize Hydraulic Fracturing Operation in a Well in the Southwest of Iran Using FracCADE Software

Amin Ahmadi , **Amir Hossein Saeedi Dehaghani*** , **Asieh Hafezi**

1. Department of Petroleum Engineering, Faculty of Chemical Engineering, Tarbiat Modares University, Tehran, Iran. E-mail: amin_ahmadi@modares.ac.ir
2. Department of Petroleum Engineering, Faculty of Chemical Engineering, Tarbiat Modares University, Tehran, Iran. E-mail: asaeedi@modares.ac.ir
3. Department of Chemistry and Chemical Engineering, Rasht Branch, Islamic Azad University, Rasht, Iran. E-mail: a.hafezi@phd.iaurasht.ac.ir

ARTICLE INFO	ABSTRACT
Article History: Received: 11 August 2022 Revised: 21 December 2024 Accepted: 06 January 2025 Published: 08 January 2025 **Article type**: Research **Keywords**: FracCADE Software, Fracturing Fluid, Hydraulic Fracturing, Proppant, Well Stimulate	Hydraulic fracturing is among the most extensively utilized techniques for enhancing hydrocarbon production in oil and gas wells, primarily by creating high permeability. These conductive flow pathways improve the well's productivity index. This study examines key factors influencing hydraulic fracturing performance, focusing on formation damage, fluid selection, and proppant optimization. Reservoir characterization was conducted using log data, enabling the division of the reservoir into three distinct zones based on their petrophysical and geo-mechanical properties. The effects of fracturing fluid composition, proppant type, and density on fracture performance were systematically investigated. Using advanced modeling tools, critical input parameters, including well completion type, fluid properties, bottom-hole pressure, and temperature, were utilized to simulate the hydraulic fracturing operation. The simulation evaluated user-controlled variables such as fluid type and volume, proppant characteristics, pump scheduling, and fracture geometry. Through iterative optimization, the study identified an optimal hydraulic fracturing design comprising 12 pumping stages. This included using Prime FRA fluid in the pad stage, YF550HT fluid in the main fracturing stages, and a 2% KCl solution for flushing. The resulting fractures exhibited an optimal length and width of 388 ft and 0.02 ft, respectively. These findings underscore the critical role of simulation in designing and optimizing hydraulic fracturing operations for enhanced reservoir performance.

Introduction

Stimulation techniques for low-permeability reservoirs with low production rates have been extensively developed to enhance oil recovery from hydrocarbon wellbores. These approaches are broadly categorized into well-centered, facilities-centered, and reservoir-centric methods [1]. Among these, hydraulic fracturing (HF) and extensive acidizing are recognized as the most effective strategies for improving the productivity of low-permeability or damaged reservoirs. Enhancing fluid flow conductivity within the reservoir rock is fundamental for increasing hydrocarbon recovery, with HF as a critical method. By propagating artificial fractures within the reservoir matrix, HF significantly improves fluid mobility. Given the extremely low

---

* Corresponding Author: A.H. Saeedi Dehaghani (E-mail address: asaeedi@modares.ac.ir)

permeability of reservoir matrices, HF is indispensable for unconventional formations and remains a cornerstone of modern reservoir stimulation practices [2-7].

Accurate pore pressure prediction is essential in hydraulic fracturing operations, particularly in geologically complex regions. Precise estimation of pore pressure informs the selection of appropriate drilling parameters, enhances wellbore stability, and mitigates risks associated with abnormal pressure zones [8]. Incorporating accurate pore pressure predictions into hydraulic fracturing designs is vital for optimizing fracture propagation

models and ensuring the safety and efficiency of stimulation operations. Understanding the interplay between pore pressure and fracture mechanics enables engineers to enhance hydrocarbon recovery while minimizing operational risks.

The simulation of HF operations is integral to stimulation engineering, facilitating the design and optimization of field applications. This study modeled HF operations using the commercial software FracCADE [9-10]. In-situ stress values, a key input for the software, were estimated due to the lack of direct measurements such as mini-frac, LOT, and XLOT tests in Iranian hydrocarbon wells. Typically performed during drilling, these tests are instrumental in determining in-situ stresses and estimating rock tensile strength when laboratory data is unavailable [11-12]. Additionally, the study incorporates a comparative analysis of simulation results with empirical relations to validate the optimized HF design.

The Perkins-Kern-Nordgren (PKN) model, a 2D geometric framework, is widely used to examine treatment design fracture propagation behavior [13]. The PKN model assumes a fixed fracture height, an elliptical vertical cross-section, and a maximum fracture width at the wellbore. As described by this model, fracture geometry is influenced by parameters such as fluid injection rate, fracturing fluid properties, rock geo-mechanical characteristics, and reservoir pressure [14]. Knudsen's evaluation of the PKN model demonstrated that fracture width is controlled by the pressure drop of the fluid within the fracture, which increases with higher fluid injection rates [15].

Riley et al. employed analytical solutions to identify fracture characteristics using well-test diagrams, addressing vertical finite conductivity fractures with elliptical cross-sections [16]. Clark pioneered a technique for estimating fracture lengths based on pressure fall-off test data, elucidating crack initiation and propagation due to hydraulic pressure [17]. Hubbert and Willis conducted seminal research on HF mechanics, establishing methodologies for determining the orientation and magnitude of principal stresses through HF processes [18].

Subsequent investigations have furthered the understanding of HF mechanics. Song et al. conducted laboratory experiments on sandstone samples to explore the relationship between fracture pressure and confining stresses in high-porosity sandstones [19]. De Pater examined HF in naturally fractured rocks, demonstrating that low-rate fluid injection leads to flow within natural fractures, whereas higher rates generate new fractures [20]. Carvalho et al. utilized finite element numerical modeling to analyze vertical HF propagation, investigating the influence of material properties on HF pressure propagation [21]. Computational methods, finite element analyses, and benchmarks from mechanical engineering have also contributed to advancing HF modeling and its practical applications [22-25].

Recent studies have introduced innovative approaches to HF modeling and optimization. For instance, a recent study presented a numerical simulation framework for optimizing fracturing technology in unconventional dense oil reservoirs, providing theoretical and practical guidance for field applications [26]. Another research focused on the simulation and optimization of unstable dynamic propagation of hydraulic fractures, offering insights into stress interactions during multiple fracturing processes [27]. Additionally, advancements in intelligent hydraulic

fracturing within the context of Industry 4.0 have been explored, emphasizing automation and innovative technologies in fracturing operations [28].

This study aims to address critical gaps in HF optimization for a well in southwestern Iran by simulating operations with FracCADE software. Key factors analyzed include injection fluid type and volume, proppant type and mass, pump scheduling, and fracture modeling. By integrating recent developments in HF mechanics and conducting comparative analyses with empirical models, this research seeks to optimize HF design and provide actionable insights for enhancing recovery efficiency in low-permeability reservoirs.

Materials and Methods

Before planning the hydraulic fracturing (HF) operation for wells in southwestern Iran, a comprehensive data set was collected, including rock mechanics, reservoir, perforation, well completion, proppant, and fracturing fluid properties. This information was sourced from previously acquired datasets. The FracCADE simulator was employed to model the HF operation in the target well. The PKN model was chosen for simulating fracture geometry, as it is particularly suited for scenarios where the fracture length (or depth) greatly exceeds the fracture height ($x_f \gg h_f$) [10].

Evaluation of Geo-mechanical Properties of Rock

Dynamic properties of rock were used to estimate Young's Modulus (E) and Poisson's ratio (v) using Eqs. 1 & 2 [29-31]:

$$E = \frac{\rho V_s^2 (3V_p^2 - 4V_s^2)}{V_p^2 - V_s^2} \tag{1}$$

$$v = \frac{(V_p^2 - 2V_s^2)}{2(V_p^2 - V_s^2)} \tag{2}$$

where E, v, V_P, and V_S are Young's Modulus, Poisson's ratio, P-wave velocity, and S-wave velocity, respectively. Most of the hydrocarbon reservoirs are carbonates. Most hydrocarbon reservoirs, including the studied site, are carbonate rocks, which are predominantly cemented. The high value of Young's Modulus, combined with the absence of wellbore collapse (based on caliper log analysis), indicates that the reservoir rock is cemented. Consequently, Biot's coefficient for cemented sedimentary rocks was calculated using Eq. 3 [32].

$$\alpha = 1 - (1 - \emptyset)^{3.8} \tag{3}$$

where α and are Biot's coefficient [-] and porosity [-], respectively.

To assess the brittleness of the reservoir rock, the method proposed by Rickman et al. [33] was applied with the following equations.

$$YM_{BRIT} = \frac{YMS - 1}{8 - 1} \times 100 \tag{4}$$

$$PR_{BRIT} = \frac{PR - 0.4}{0.15 - 0.4} \times 100 \tag{5}$$

$$BRIT = \frac{YM_{BRIT} + PR_{BRIT}}{2} \tag{6}$$

YM$_{BRIT}$, PR$_{BRIT}$, BRIT, YMS, and PR are Young's Modulus brittleness [-], Poisson's ratio brittleness [-], brittleness of reservoir rock [-], Young's Modulus (psi), and Poisson's ratio, respectively.

After the fracturing treatment, proppant injection is essential to prevent fracture closure, thereby enhancing the productivity index. The effectiveness of the proppant depends on the volume injected, the permeability ratio between the proppant and reservoir, and the induced fracture geometry. These factors are expressed in terms of dimensionless fracture direction (C$_{fD}$) and influx ratio (I$_x$) [34].

$$C_{fD} = \frac{k_f w}{k x_f} \tag{7}$$

$$I_x = \frac{2x_f}{x_e} \tag{8}$$

C$_{fD}$, I$_x$, k$_f$, w, k, x$_f$, and x$_e$ are dimensionless fracture direction, influx ratio, fracture permeability (mD), fracture Width (ft), reservoir permeability (mD), fracture length (ft), and drainage area radius (ft), respectively.

The dimensionless number of proppants is defined using the dimensionless fracture direction and influx ratio [34].

$$N_{prop} = \frac{2k_f V_p}{k V_r} = I_x^2 \times C_{fD} \tag{9}$$

The productivity index (J) is used to quantify the reservoir's fluid flow capacity, and it is calculated as the ratio of a well's flow rate to the pressure drop between the reservoir and bottom hole, defined by [35]:

$$J = \frac{q}{P_{ave} - P_{wf}} \tag{10}$$

The dimensionless productivity index (J$_D$) is calculated by Eq. 11 [36].

$$J_D = \frac{1}{\ln\left(0.472\frac{r_e}{r_w}\right) + S'} \tag{11}$$

Where J, J$_D$, q, P$_{ave}$, P$_{wf}$, r$_e$, r$_w$, and s' are productivity index (bbl/day/psi), dimensionless productivity index, flow rate (bbl/day), average reservoir pressure (psi), bottom hole pressure (psi), reservoir radius (in), well radius (in) and pseudo skin factor, respectively.

The HF operation was simulated using FracCADE 5.1 software. The input parameters for the simulation are detailed in the tables below.

Table 1. Primary good information for FracCADE input

Well depth (ft)	Well diameter (ft)	Proppant injection method	Static bottom-hole temperature (F)	Surface temperature (F)	Packer depth (ft)	Packer diameter (in)
11023	7	Piping	220	80	10481	7

In Table 2, the information related to the completion of the well is entered from the available data. According to the available information, the type of piping in the desired well is complete.

Then, the information about the casing is reported in Table 3, along with the available information about the well. According to Table 4, the actual vertical depth (TVD) and measured depth (MD) are equal due to the verticality of the well.

Table 2. Piping information

Name	Total depth (ft)	Outer diameter (in)	Inner diameter (in)	Weight (lb/ft)	Outer pressure (psi)	Inner pressure (psi)
N80	10581	4.5	3.830	15.5	11085	10484

Table 3. Casing information

Inner pressure (psi)	Outer pressure (psi)	Weight (lb/ft)	Inner diameter (in)	Outer diameter (in)	Total depth (ft)	Name
3060	1500	133	18.730	20	193	K55
7560	4180	80	12.159	13.375	6007	C95
9090	8660	61	8.375	9.625	7939	N80
9240	10180	35	6.004	7	11023	N80

Table 4. Perforation information

Top MD (ft)	Top TVD (ft)	Bottom TVD (ft)	Bottom MD (ft)	Perforation density (shots/ft)	Number of perforations	Perforation diameter (in)	Tunnel length (in)
9581.1	958.1	10581.3	10581.3	0	0	0	8
10581.3	10581.3	10758.4	10758.4	0.47	84	84	8
10758.4	10758.4	11020.2	11020.2	0.5	131	131	8

Table 5. Zone information

	Zone 1	Zone 2	Zone 3
Lithology	Shale	Carbonate	Carbonate
Layer MD (ft)	9985.1	10581.3	10758.4
Layer TVD (ft)	9985.1	10581.3	10758.4
Reservoir height (ft)	623.2	177.1	261.8
Net layer thickness (ft)	623.2	177.1	261.8
Number of perforations	0	84	131
Perforation diameter (in)	0	0.33	0.33

Table 6. Zone Porosity and Permeability information

	Zone 1	Zone 2	Zone 3
Porosity %	1	18.6	14
Permeability (MD)	0.001	2.5	2.5
Fracture pressure gradient (psi/ft)	0.777	0.683	0.683
Min in-situ stress (Psi)	7975	7264	7434
Reservoir pressure (Psi)	4300	4200	4320
Young's Modulus (Psi)	3.077^{+06}	3.077^{+06}	3.077^{+06}
Poisson's ratio	0.23	0.27	0.27
fracture hardness (Psi/in)	1000	1200	1200

Table 7. Fracturing fluid information

Number	Fluid compositions
1	2% KCL Water
2	105LB/K HEC w/0.4% J503+20PPT J464
3	73LB/K HEC w/8 PPT J218+ 1GPT J318
4	73LB/K HEC w/NO BREAKER
5	PrimeFRAC 30 + 1lbs J475/Mgal
6	YF550HT w/10 lb/k J353 + 10lb/k J418
7	YF550HT w/10 lb/k J353 + 15 lb/k J418

Table 8. Selected fluid additives in HF operations information

Number	Name	Specific gravity of the base fluid	Gel concentration 1b\mga1
1	2% KCL Water	1	0
2	105LB/K HEC w/0.4% J503+20PPT J464	1.01	106.2
3	73LB/K HEC w/8 PPT J218+ 1GPT J318	1.01	73
4	73LB/K HEC w/NO BREAKER	1.01	73
5	PrimeFRAC 30 + 1lbs J475/Mgal	1.02	30
6	YF550HT w/10 lb/k J353 + 10lb/k J418	1	50
7	YF550HT w/10 lb/k J353 + 15 lb/k J418	1	50

Table 9. Rheology information of selected fluids in HF operations

Number	Name	Shear rate	Viscosity	k value	n value
1	2% KCL Water	170	0.276	0.276	1
2	105LB/K HEC w/0.4% J503+20PPT J464	170	232.544	232.544	0.49
3	73LB/K HEC w/8 PPT J218+ 1GPT J318	170	227.952	227.952	0.43
4	73LB/K HEC w/NO BREAKER	170	77.993	77.993	0.65
5	PrimeFRAC 30 + 1lbs J475/Mgal	170	315.528	315.528	0.62
6	YF550HT w/10 lb/k J353 + 10lb/k J418	170	436.922	436.922	0.62
7	YF550HT w/10 lb/k J353 + 15 lb/k J418	170	436.922	436.922	0.62

Table 10. Loss of selected fluids in HF operation data

Number	Fluid name	Spontaneity loss	Fluid filter viscosity
1	2% KCL Water	2.5	1
2	105LB/K HEC w/0.4% J503+20PPT J464	0	94.7
3	73LB/K HEC w/8 PPT J218+ 1GPT J318	0	83.4
4	73LB/K HEC w/NO BREAKER	0	39.8
5	PrimeFRAC 30 + 1lbs J475/Mgal	2.8	1
6	YF550HT w/10 lb/k J353 + 10lb/k J418	1.1	1
7	YF550HT w/10 lb/k J353 + 15 lb/k J418	0.6	1

Table 11. Selected proppants

Number	Proppant name	Permeability	Specific gravity	Porosity	Mean particle diameter	Mesh size
1	Sand	36235	2.65	35	0.025	20.40
2	12/20 PRB	161400	2.53	35	0.039	12.20
3	20/40PRB	91063	2.53	35	0.028	20.40
4	12/20 Brady	30856	2.65	35	0.048	12.20
5	20/40 Brady	24225	2.65	35	0.023	20.40
6	12/20 Carbo	295076	3.25	35	0.041	12.20
7	20/40 Carbo	227983	3.35	35	0.025	20.40

Result and Discussion

Log Data Analysis

Comprehensive log data analysis was conducted on a well located in southwestern Iran, employing spectral gamma-ray (SGR), micro-spherical focused log (MSFL), shallow resistivity (LLS), deep resistivity (LLD), sonic wave, density, and neutron logs. This extensive approach provided a holistic understanding of the reservoir characteristics and allowed for precise interval characterization.

Interval 9958–10581 ft

The gamma-ray log (Fig. 1a) exhibits high readings, indicating elevated shale content and extremely low permeability. Sonic log (DT) measurements further confirm a high clay content and elevated water saturation. Increased P-wave velocities observed within this interval highlight the presence of a dense, low-porosity matrix with minimal fluid storage capacity. Wellbore stability was assessed using caliper log data, revealing no significant issues such as clay swelling or borehole collapse, which is critical for the integrity of drilling operations. Neutron log data corroborate the low porosity findings, strengthening understanding the formation's compact nature. Resistivity logs (MSFL, LLS, LLD) exhibit high water saturation and limited permeability, with MSFL showing consistently higher resistivity than LLS and LLD. This contrast suggests significant salinity differences between the reservoir water and the drilling fluid, emphasizing the need for specialized techniques to evaluate potential productivity.

Interval 10581–10758 ft

Gamma-ray log readings (Fig. 1b) remain elevated, reflecting substantial shale content and associated water saturation throughout this interval. Despite these findings, certain zones exhibit anomalies indicative of hydrocarbon presence, particularly at depths of 10555–10578 ft and 10594–10627 ft. These zones are characterized by deviations in resistivity logs, signaling localized permeability enhancements. This interpretation is further supported by lower-density log values, which align with consistent neutron log readings pointing to higher porosity. The lower segment of this interval (16–32 ft) is particularly notable as a promising hydrocarbon-bearing zone. These findings underscore the heterogeneity of the formation and its potential for selective exploitation.

Interval 10758–11023 ft

The target reservoir (Fig. 1c), spanning 475 ft, presents highly favorable characteristics, including high porosity, substantial permeability, and significant hydrocarbon saturation. This interval was prioritized for hydraulic fracturing operations due to its optimal conditions. Detailed analysis of the petrophysical properties in this section supports the selection of this zone, as it represents the most promising area for maximizing hydrocarbon recovery within the analyzed intervals. The interplay between the formation's mechanical and fluid storage properties further strengthens its potential as a key production zone.
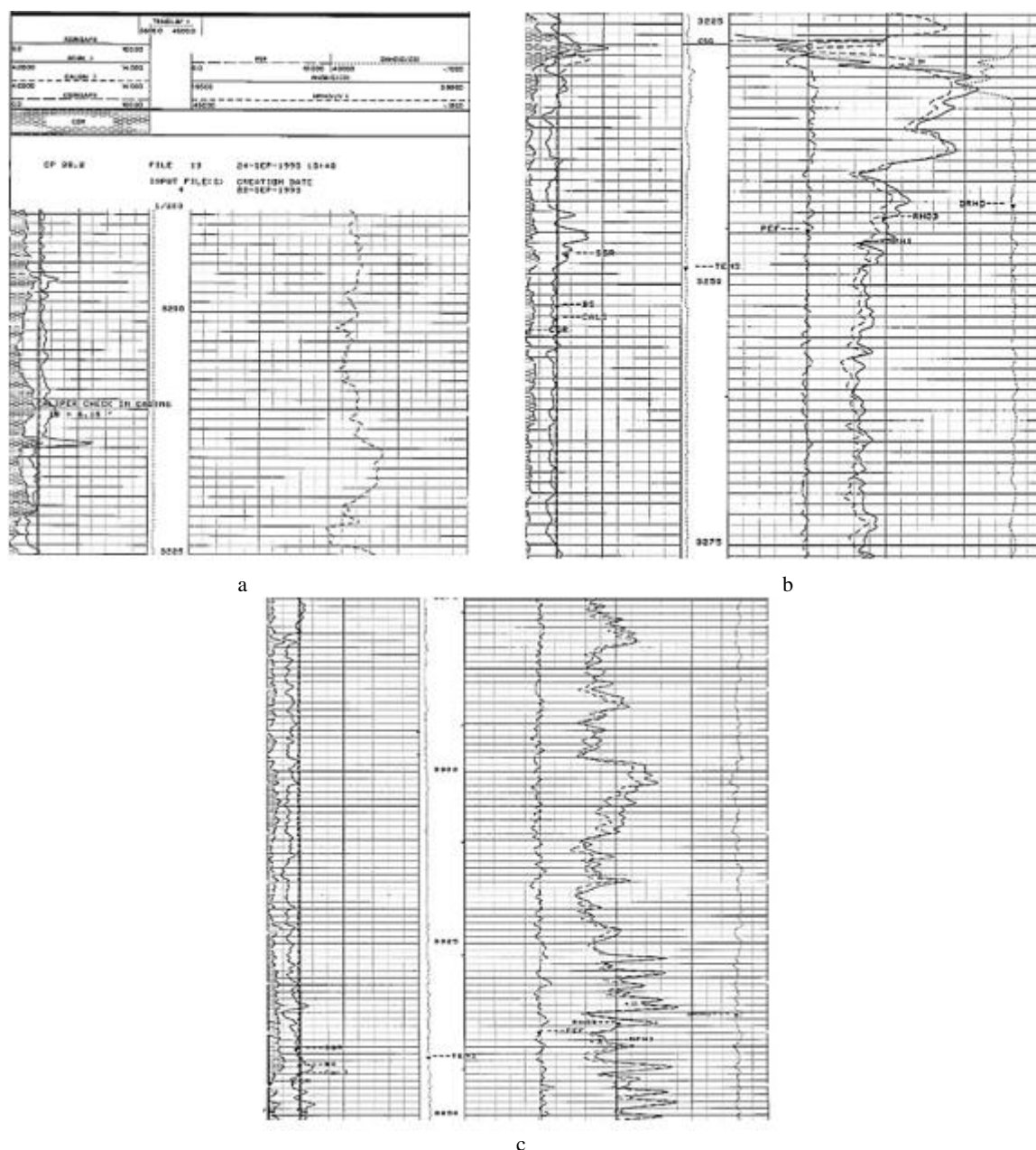
Fig. 1. Gamma logs and porosity logs related to the range (a) 9958-10581, (b) 10581-10758, and (c) 10758-11023 ft

All the used gases had a purity of ≥ 99.99%. Feed gas was used at a 100 mL/min flow rate, which included the following percentages (v/v): 5% helium, 10% nitrogen, 15% carbon dioxide, and 70% methane.
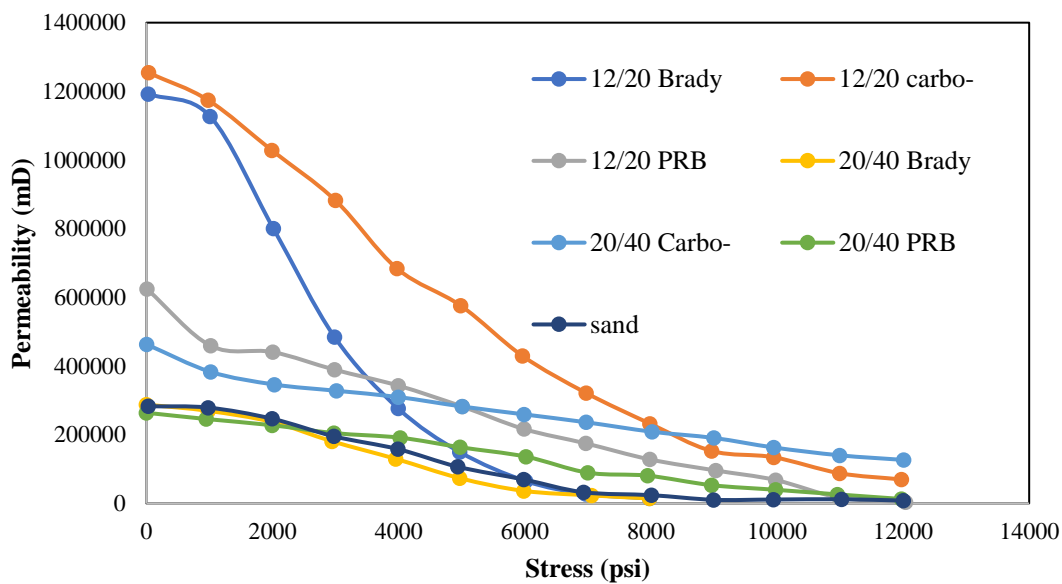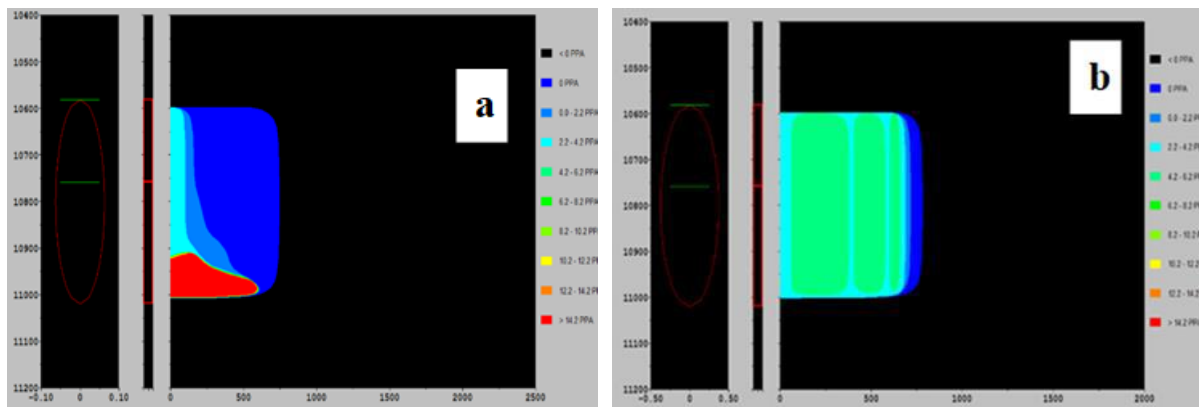
Geo-mechanical Properties

Key geo-mechanical parameters such as Young's Modulus, Poisson's ratio, Biot's coefficient, and brittleness were derived from well log data and tabulated (Table 12). These properties formed the basis for FracCADE simulations, ensuring an informed approach to hydraulic fracturing design and optimization.

Table 12. Young's Modulus (E), Poisson's ratio, Biot's coefficient, and brittleness of reservoir rock

Depth (ft)	Poisson's ratio	E (million psi)	Vs (m/s)	Vp (m/s)	Dt (us/ft)	bulk density (g/cc)	BRIT (%)	PR_BRIT (%)	YM_BRIT (%)	Biot's coefficient (%)
9840	0.29	6.583	2615	4801	63.5	2.54	61.8787	44	79.75	0.33
10660	0.27	4.638	2289	4065	75	2.375	51.98	52	51.97	0.592
10824	0.29	6.86	2661	4917	62	2.55	63.87	44	83.75	0.411
11023	0.29	6.86	2661	4917	62	2.55	63.87	44	83.75	0.436

Fracture Simulation Results

FracCADE simulations were employed to optimize fracture design parameters. Critical outcomes include insights into proppant permeability under varying pressure conditions (Fig. 2) and the distribution of proppant concentrations along fracture lengths (Fig. 3). The analysis highlights the pivotal role of fluid viscosity in ensuring efficient proppant transport. Suboptimal viscosity levels (Fig. 3a) lead to proppant settling near the fracture initiation point, compromising uniform distribution.

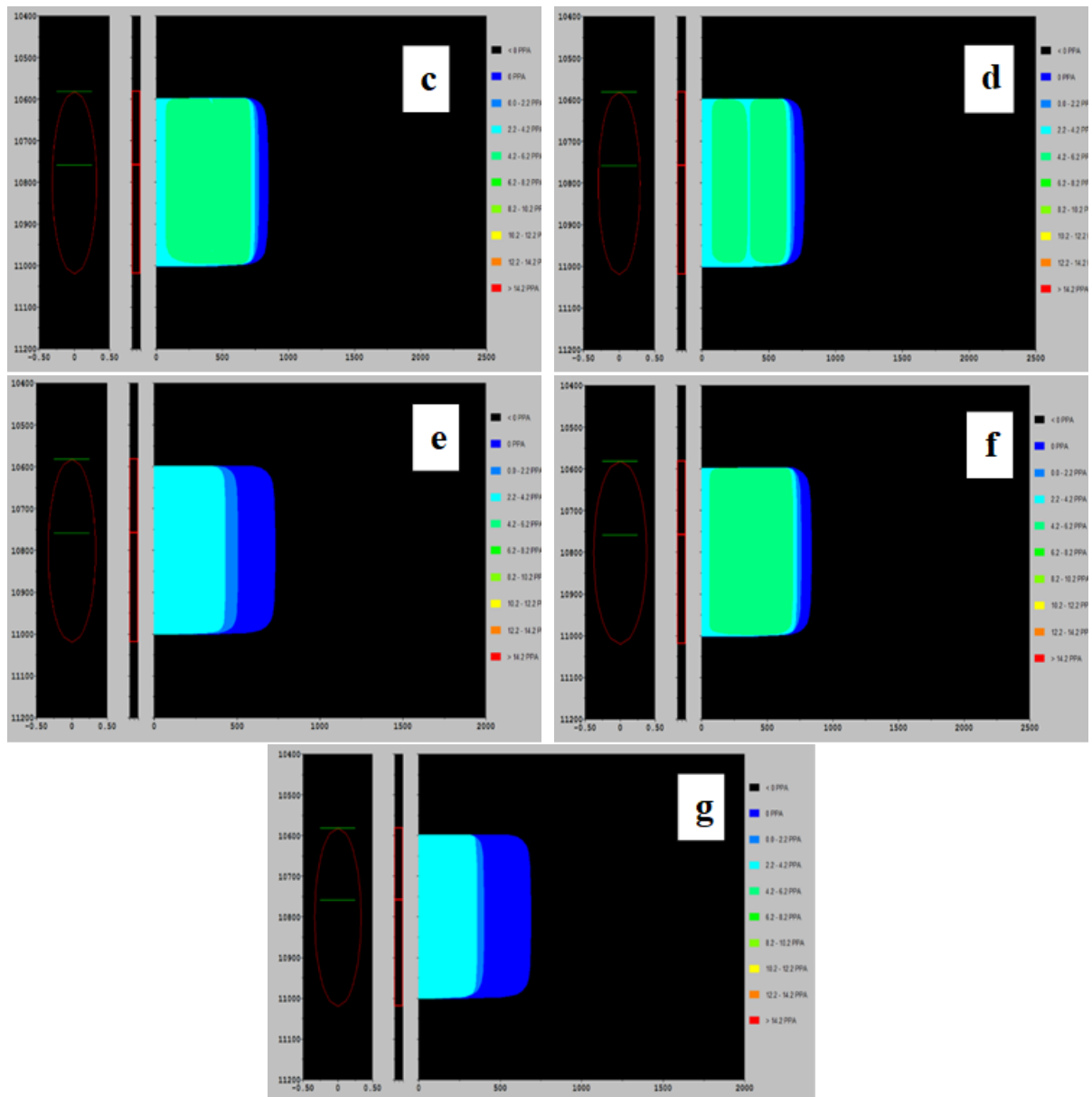**Fig. 2**. Permeability of the selected proppants

Fig. 3. Proppant concentration diagram along the length of the fracture when the fracturing fluid is (a) number 1, (b) number 2, (c) number 3, (d) number 4, (e) number 5, (f) number 6, and (g) number 7, according to Table 7

Pressure and Temperature Dynamics

Injection operations demonstrated a progressive increase in bottom-hole pressure over time (Fig. 4). Concurrently, the injection of cooler pad fluids resulted in an initial temperature drop from 220°F to 80°F. Subsequent frictional heating during proppant injection led to a temperature rebound (Fig. 5).
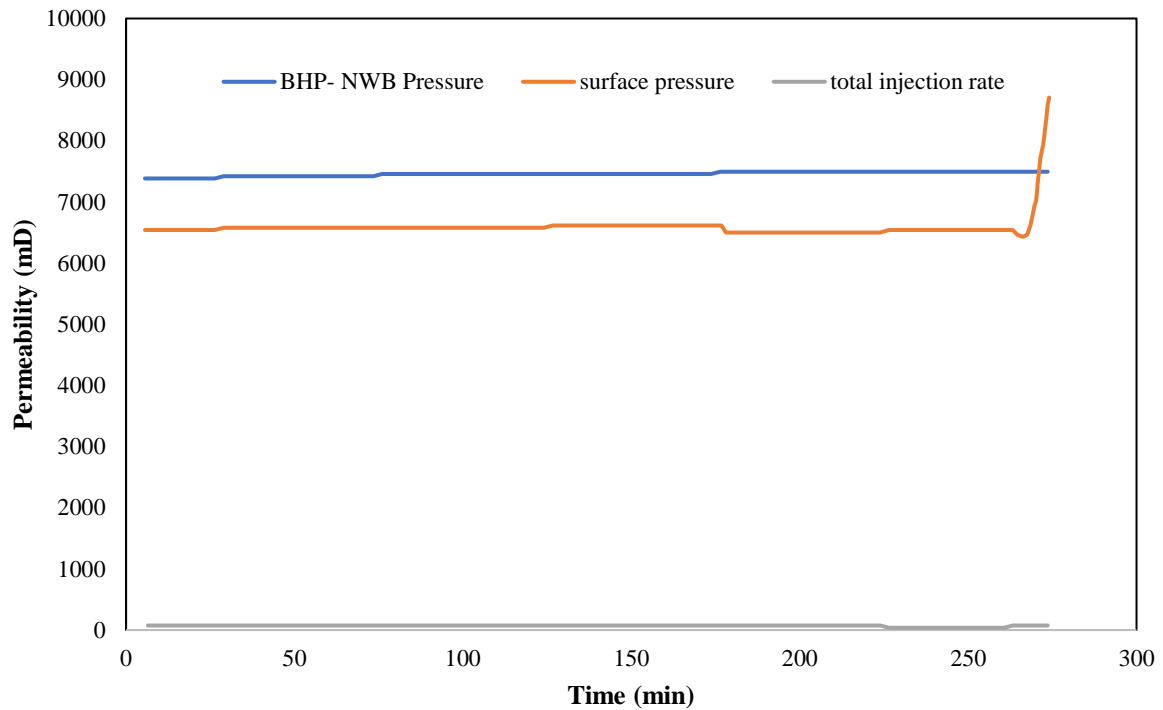
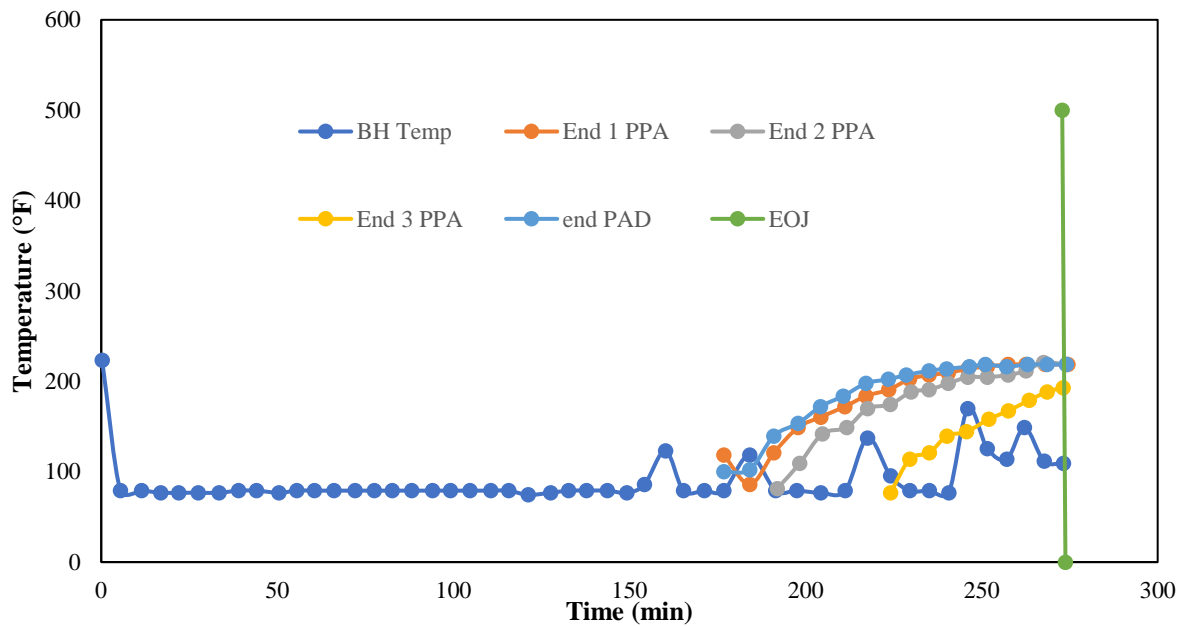**Fig. 4**. Bottom hole pressure and surface pressure

Fig. 5. Temperature vs. time

Fracture Length and Proppant Distribution

Fracture half-length (Fig. 6) and proppant concentration profiles (Fig. 7) underscore the effectiveness of optimal fluid-proppant combinations. Proppant concentration diminishes with increasing distance from the well, consistent with the intended fracture geometry. This highlights the importance of tailored fracturing fluid properties to achieve the desired distribution. Fig. 7a & b are 3D and 2D outputs of the proppant concentration at half-length of

the fracture, showing that the proppant concentration decreases as it moves away from the well. It has been designed for the well's vertical depth and the fracture's length.
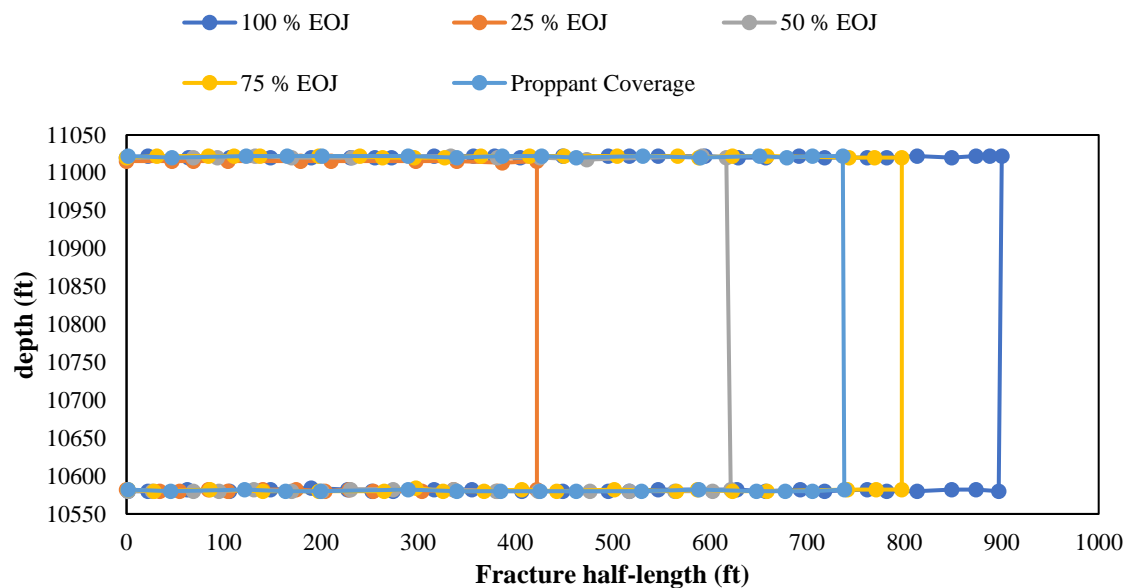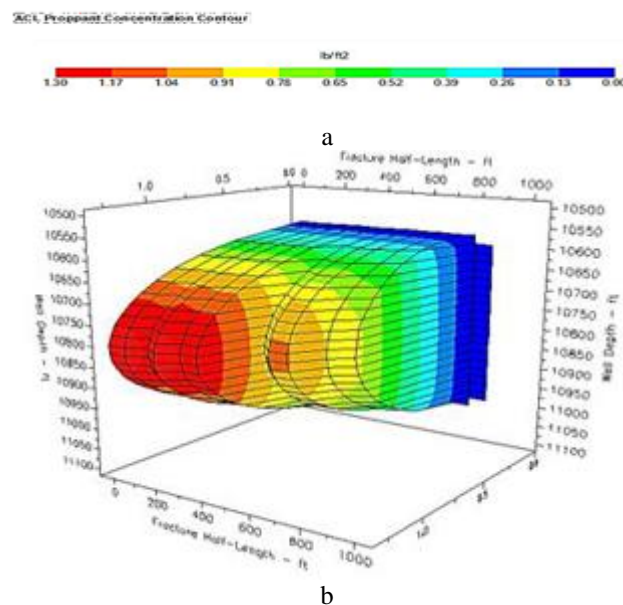

Fig. 6. Fracture length at the end of the job (EOJ)

Fig. 7. 2D (a) and 3D (b) output of the proppant concentration at half-length of the fracture

Hydraulic Fracture Design and Optimization

The reservoir volume, calculated for a well drainage area of 160 acres, was determined to be 6,969,600 ft³ per unit thickness. Y550HT fracturing fluid was selected for its exceptional thermal stability and polymeric structure, which facilitates superior proppant transport compared to initial trials with brine and GUAR mixtures, which proved inadequate. This choice reflects the critical role of fluid design in achieving optimal fracturing outcomes.

Sixteen simulations evaluated varying proppant volumes, fluid types, and pumping schedules (Table 14). The optimal parameters were identified by aligning simulated results with theoretical dimensionless fracture conductivities (CfD). Simulation 16 achieved the best

correlation (Table 14, Fig. 8), resulting in the desired fracture dimensions and proppant placement. These findings highlight the iterative nature of the optimization process and the importance of integrating theoretical and simulation-based approaches.

Table 13. Types and specifications of selected proppants

Proppant type	Permeability (mD)	Porosity	MW	Mesh size
Sand covered with resin	201576	0.35	2.53	12/20
Sand covered with resin	109277	0.35	2.53	20/40

Table 14. Outputs of 16 simulations with FracCADE

Simulation	N_{prop}	$C_{fD,Opt}$ Theory	$x_{f,Opt}$	$w_{f,Opt}$	$J_{D,Opt}$	$C_{fD,Sim}$	$N_{prop, Sim}$	$C_{fD,Opt\ Sim}$	$x_{f,Sim}$	$w_{f,Sim}$	$J_{D,Opt}$
1	1.13	4	701.153	0.01789	0.9	18.6	11.457	20	398.5	0.522	1.6
2	0.22	2	433.739	0.01446	0.55	14.8	8.3363	15	392.5	0.182	1.6
3	0.97	3	750.008	0.00836	0.75	4.9	7.40833	8	506.4	0.111	1.3
4	0.59	2.8	604.785	0.00518	0.65	7.8	8.204715	9	502.7	0.015	1.4
5	0.58	2.7	613.928	0.00511	0.6	5.4	8.003296	8.8	502.1	0.086	1.2
6	0.1	1.6	338.615	0.00926	0.4	1.1	2.05164	3	435.4	0.095	0.8
7	0.13	2	335.28	0.011	0.5	1.3	2.7091	4	433.3	0.107	0.9
8	0.006	1.6	83	0.004	0.27	0.4	0.205761	1.5	195	0.02	0.5
9	0.02	1.6	131.6	0.004	0.32	2.4	0.106508	2	121.5	0.065	1.1
10	0.085	1.6	305.16	0.009	0.3	13.1	0.509192	13	104.2	0.298	0.5
11	0.14	1.3	426	0.01	0.55	1.9	0.535	2.2	397.9	0.15	0.7
12	0.19	2.2	390.6	0.01	0.6	1.7	0.5	3	405	0.11	0.65
13	0.26	2.5	424.46	0.014	0.5	2.4	0.7	3.3	404	0.149	0.7
14	0.54	4	485	0.02	0.6	12.2	1.36	6	251	0.5	1.1
15	0.19	2.2	368	0.01	0.5	1.9	0.44	2.5	361	0.11	0.7
16	0.19	2.2	388	0.016	0.5	2.2	0.53	4.5	367	0.197	0.7

In Table 14, we enter a specific proppant mass and calculate the proppant mass per unit of reservoir thickness for each simulation. Then, we enter the volume of different fluids for each simulation. Using different pumping programs and the type of proppant and fluid we have selected, we calculate the proppant number for each simulation with Eq. 9. After calculating CfD through Eq. 7, we have to calculate the fracture length (W_f) and the fracture's width (X_f) using Eqs. 12 & 13 [37].

$$x_{f\ opt} = (\frac{k_f V_p}{C_{fD\ opt} kh})^{0.5} \qquad (12)$$

$$w_{f\ opt} = (\frac{C_{fD\ opt} k V_p}{k_f h}) \qquad (13)$$

Where $w_{f.opt}$, $x_{f.opt}$, $C_{fD.opt}$, k_f, k, h, V_p are the fracture's length, the fracture's width, dimensionless fracture direction [-], fracture permeability (mD), reservoir permeability (mD), thickness (ft), and proppant volume (ft^3), respectively.

After the simulation, the C_{fD} obtained in each simulation should be compared with the C_{fD} obtained from the theory. If the C_{fD}s are matched, the design has been optimized. We have listed 16 simulations as examples of all simulations taken in Table 14; in each simulation, the mass of the proppant, type of fluid, and the fluid pumping plan have changed. It should be noted that no specific trend was observed in these changes, and we have achieved our desired result by taking many simulations. Based on the calculations performed, we checked the 16 simulations identified in Table 14. According to the optimization conditions, we have selected simulation 16, that the C_{fD} of the simulator is equal to the C_{fD} of the theoretical method, as the optimal operation. According to Table 14 and Fig. 8, we chose the simulation number (16) as our optimal design; the various specifications can be seen in Table 14. Optimized parameters and FracCADE outputs are compared in Fig. 8.

Table 15. Pumping stages for simulation 16

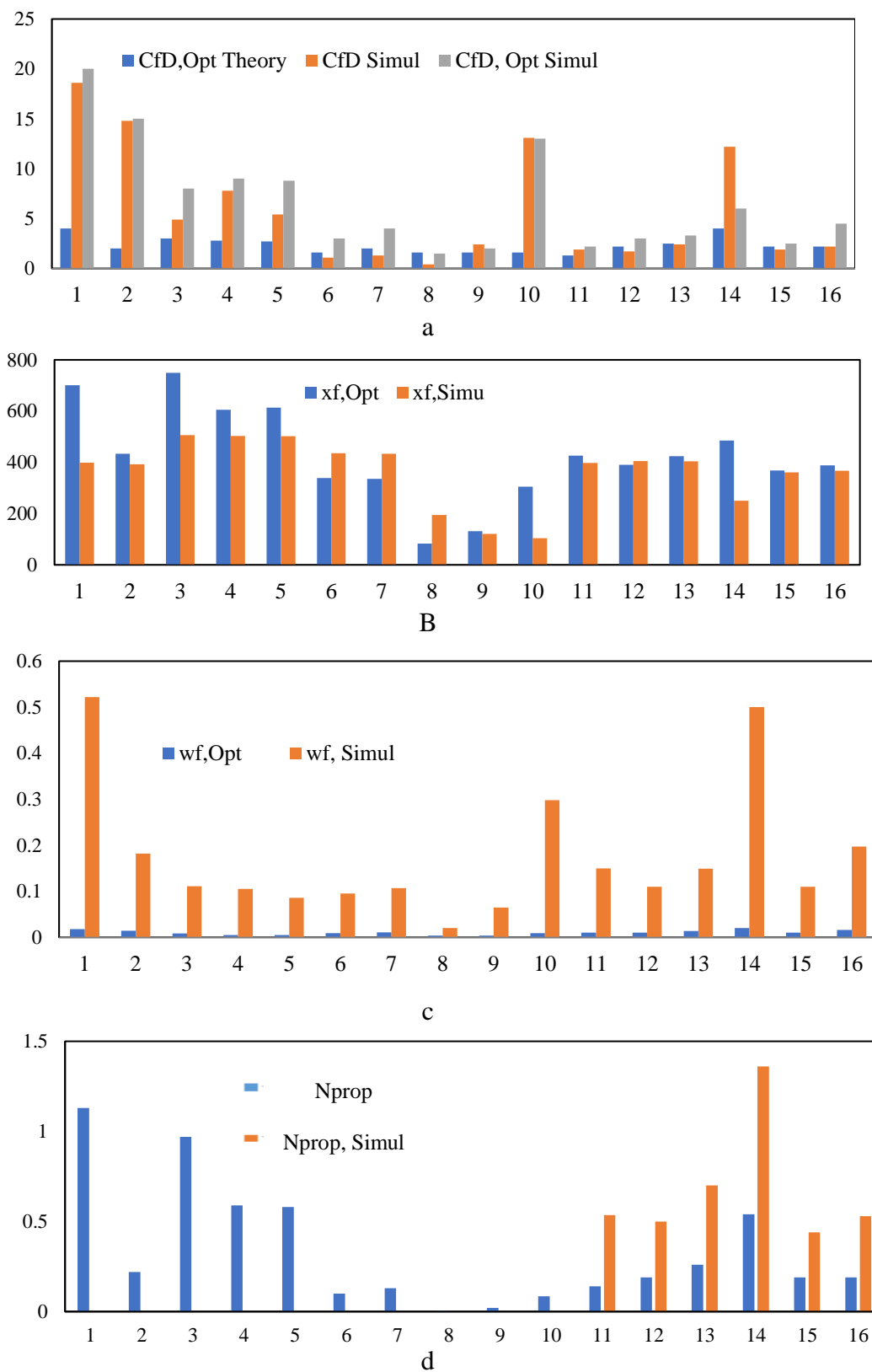|	Stage name	Fluid number	Fluid name	Pumping time (min)	Proppant weight	Proppant density	Proppant number	Fluid volume	Gel concentration
1	pad	5	PrimeFRA	198	0	0	0	249649	25
2	1 PPA	6	YF550HT	4.8	7826	1	3	7693	50
3	4 PPA	6	YF550HT	4.8	27019	4	3	6763	50
4	5 PPA	6	YF550HT	7.8	53545	5	3	10547	50
5	7 PPA	6	YF550HT	7.8	65615	7	3	9975	50
6	8 PPA	6	YF550HT	7.8	77234	8	3	9446	50
7	10 PPA	6	YF550HT	7.8	87650	10	3	8932	50
8	11 PPA	6	YF550HT	3.9	48184	11	2	4270	50
9	12 PPA	6	YF550HT	3.9	50117	12	2	4157	50
10	13 PPA	6	YF550HT	5.9	78418	13	2	6114	50
11	14 PPA	6	YF550HT	5.8	82238	14	2	5912	50
12	flush	1	2% KCl w	5	0	0	0	6345	0

Fig. 8. Theoretical and simulated C_{fD} (a), (b) x_f (b), (c) w_f (c), and N_{prop} (d)

Conclusion

The simulation of hydraulic fracturing (HF) processes is a critical prerequisite for successful operations, particularly given the unique characteristics of each well and reservoir. This study focused on simulating HF operations for a well in southwestern Iran using the FracCADE software. Various designs involving different proppants and fracturing fluids were modeled to evaluate their impact on fracture propagation and overall reservoir performance. Key parameters, including proppant density, particle size, and fluid type, were systematically analyzed to optimize the fracturing process before actual injection.

The simulations provided valuable insights into the spatial distribution of proppant concentrations within fractures and the dynamics of fracture opening under varying conditions. By iteratively refining the design, multiple simulations were conducted, and the most effective results were identified based on both theoretical calculations and software outputs. Simulation number 16 emerged as the optimal design, demonstrating excellent alignment between theoretical models and FracCADE results.

The optimized design incorporates 12 pumping stages, meticulously tailored to maximize efficiency and ensure effective proppant placement. This includes:

1. Pad Stage: A single pumping step employing PrimeFRA fluid over 198 minutes to establish initial fracture geometry and create a clean fracture pathway.
2. Particle-Plugging Stages: Ten consecutive pumping steps utilizing YF550HT fluid, chosen for its superior proppant transport capabilities and thermal stability.
3. Flush Stage: A final pumping step using a 2% KCl fluid solution over 5 minutes to displace residual proppants and stabilize the fracture network.

This comprehensive approach underscores the importance of integrating advanced simulation tools and iterative optimization in the design of HF operations. This study provides a blueprint for enhancing production outcomes in low-permeability reservoirs by leveraging robust numerical analyses and software simulations.

References

[1]   Zoback, MD (2007) Reservoir Geomechanics/Cambridge, New York, Melbourne: Cambridge University Press. DOI: https://doi.org/10.1017/CBO9780511586477.

[2]   Economides, Michael J, A practical companion to reservoir stimulation. 1992: Elsevier. DOI: https://lib.ugent.be/catalog/ebk01:1000000000556275.

[3]   Pang, Yu, Mohamed Y Soliman, Hucheng Deng, and Hossein Emadi (2017) Analysis of effective porosity and effective permeability in shale-gas reservoirs with consideration of gas adsorption and stress effects, SPE journal. 22(06). 1739-1759. DOI: http://dx.doi.org/10.2118/180260-PA.

[4]   Guo, Tiankui, Songjun Tang, Shun Liu, Xiaoqiang Liu, Jianchun Xu, Ning Qi, and Zhenhua Rui (2021) Physical simulation of hydraulic fracturing of large-sized tight sandstone outcrops, SPE journal. 26(01). 372-393. DOI: http://dx.doi.org/10.2118/204210-PA.

[5]   Heider, Yousef (2021) A review on phase-field modeling of hydraulic fracturing, Engineering Fracture Mechanics. 253. 107881. DOI: https://doi.org/10.1016/j.engfracmech.2021.107881

[6]   Sun, Shanhui, Meihua Zhou, Wei Lu, and Afshin Davarpanah (2020) Application of symmetry law in numerical modeling of hydraulic fracturing by finite element method, Symmetry. 12(7). 1122. DOI: http://dx.doi.org/10.3390/sym12071122.

[7]   Schultz, Ryan, Robert J Skoumal, Michael R Brudzinski, Dave Eaton, Brian Baptie, and William Ellsworth (2020) Hydraulic fracturing- induced seismicity, Reviews of Geophysics. 58(3). e2019RG000695. DOI: https://doi.org/10.1029/2019RG000695.

[8]   Ahmadi, Amin, Mohsen Saemi, Alireza Shahnazi, Mohammad Hossein Shahmoradi, and

Abdollah Molaghab (2024) Geomechanical methods for pore pressure prediction in complex geological structures: a case study of a field in southwest of Iran, Arabian Journal of Geosciences. 17(10). 283. DOI: https://doi.org/10.1007/s12517-024-12093-1.

[9] Sulistyarso, Harry Budiharjo (2019) Effect of Pump Rate Penetration Sensitivity on Hydraulic Fracturing in Low Resistivity Reservoir. DOI: https://doi.org/10.11648/j.pse.20190301.13.

[10] Ramadhan, Dimas, Hidayat Tulloh, and Cahyadi Julianto (2020) Analysis Study of The Effect in Selecting Combination of Fracturing Fluid Types and Proppant Sizes On Folds Of Increase (FOI) To Improve Well Productivity, Journal of Petroleum and Geothermal Technology. 1(2). 92-99. DOI: http://dx.doi.org/10.31315/jpgt.v1i2.3886.

[11] Osiptsov, Andrei A (2017) Fluid mechanics of hydraulic fracturing: a review, Journal of Petroleum Science and Engineering. 156. 513-535. DOI: http://dx.doi.org/10.1016/j.petrol.2017.05.019.

[12] Wang, Zhiqi, Qingjie Guo, Xinmin Liu, and Changqing Cao (2007) Low temperature pyrolysis characteristics of oil sludge under various heating conditions, Energy & Fuels. 21(2). 957-962. DOI: http://dx.doi.org/10.1021/ef060628g.

[13] van de Poll, Student JAN and H Garikapati (2019) Bayesian inference for the PKN hydraulic fracturing model.

[14] Meyer, BR.(1986) Design formulae for 2-D and 3-D vertical hydraulic fractures: model comparison and parametric studies. in SPE Unconventional Gas Technology Symposium. OnePetro.

[15] Knudsen, MJ (2012) Extraction of Natural Gas by Hydraulic Fracturing, University of Florida. 201. 11-12.

[16] Riley, MF, WE Brigham, and RN Horne.(1991) Analytic solutions for elliptical finite-conductivity fractures. in SPE Annual Technical Conference and Exhibition. OnePetro. DOI: https://doi.org/10.2118/26912-MS.

[17] Clark, KK (1968) Transient pressure testing of fractured water injection wells, Journal of petroleum technology. 20(06). 639-643. DOI: https://doi.org/10.2118/1821-PA.

[18] Hubbert, M King and David G Willis (1957) Mechanics of hydraulic fracturing, Transactions of the AIME. 210(01). 153-168. DOI: https://doi.org/10.2118/686-G.

[19] Song, Insun, Mancheol Suh, Kyoung Sik Won, and Bezalel Haimson (2001) A laboratory study of hydraulic fracturing breakdown pressure in tablerock sandstone, Geosciences Journal. 5(3). 263-271. DOI: http://dx.doi.org/10.1007/BF02910309

[20] De Pater, CJ and LJL Beugelsdijk.(2005) Experiments and numerical simulation of hydraulic fracturing in naturally fractured rock. in Alaska Rocks 2005, The 40th US Symposium on Rock Mechanics (USRMS). OnePetro.

[21] Carvalho, Eulher C, Marko AL Bendezu, Maria FF de Oliveira, Deane M Roehl, and Luis C de Sousa Jr (2010) Finite element modeling of hydraulic fracturing in vertical wells, Mecânica Computacional. 29(88). 8571-8578.

[22] Bourdin, Blaise, Gilles A Francfort, and Jean-Jacques Marigo (2000) Numerical experiments in revisited brittle fracture, Journal of the Mechanics and Physics of Solids. 48(4). 797-826. DOI: http://dx.doi.org/10.1016/S0022-5096(99)00028-9

[23] Bourdin, Blaise, Gilles A Francfort, and Jean-Jacques Marigo (2008) The variational approach to fracture, Journal of elasticity. 91(1). 5-148. DOI: http://dx.doi.org/10.1007/s10659-007-9107-3

[24] Miehe, Christian, Fabian Welschinger, and Martina Hofacker (2010) Thermodynamically consistent phase- field models of fracture: Variational principles and multi- field FE implementations, International journal for numerical methods in engineering. 83(10). 1273-1311. DOI: http://dx.doi.org/10.1002/nme.2861.

[25] Schlüter, Alexander, Adrian Willenbücher, Charlotte Kuhn, and Ralf Müller (2014) Phase field approximation of dynamic brittle fracture, Computational Mechanics. 54(5). 1141-1161. DOI: http://dx.doi.org/10.1007/s00466-014-1045-x.

[26] Wu, Huimei, Nan Zhang, Yishan Lou, Xiaopeng Zhai, Bin Liu, and Song Li (2024)

Optimization of fracturing technology for unconventional dense oil reservoirs based on rock brittleness index, Scientific Reports. 14(1). 15214. DOI: http://dx.doi.org/10.1038/s41598-024-66114-w.

[27] Wang, Jue, Genbo Peng, Lei Zhang, Ziyuan Cong, and Buqin Hu (2024) Simulation and optimization of unstable dynamic propagation of multiple fractures in the shale formation, Frontiers in Earth Science. 12. 1394491. DOI: http://dx.doi.org/10.3389/feart.2024.1394491.

[28] Jia, Jing, Qinghu Fan, Jianglu Jing, Kehui Lei, and Lichang Wang (2024) Intelligent hydraulic fracturing under industry 4.0—a survey and future directions, Journal of Petroleum Exploration and Production Technology. 1-21. DOI: http://dx.doi.org/10.1007/s13202-024-01877-6.

[29] Miller, Susan LM and Robert R Stewart (1991) The relationship between elastic-wave velocities and density in sedimentary rocks: A proposal, Crewes Res. Rep. 260-273.

[30] Luo, Xuan, Patrick Were, Jianfeng Liu, and Zhengmeng Hou (2015) Estimation of Biot's effective stress coefficient from well logs, Environmental earth sciences. 73(11). 7019-7028. DOI: http://dx.doi.org/10.1007/s12665-015-4219-8.

[31] WurohTimbo, Mohamed, An improved methodology on wellbore stability prediction using geomechanical analysis. 2012, UNIVERSITI TEKNOLOGI PETRONAS.

[32] Bailin, Wu.(2001) Boit's effective stress coefficient evaluation: static and dynamic approaches. in ISRM International Symposium-2nd Asian Rock Mechanics Symposium. OnePetro. DOI: http://dx.doi.org/10.1201/9781003077510-85.

[33] Rickman, Rick, Michael J Mullen, James Erik Petre, William Vincent Grieser, and Donald Kundert.(2008) A practical use of shale petrophysics for stimulation design optimization: All shale plays are not clones of the Barnett Shale. in SPE annual technical conference and exhibition. Society of Petroleum Engineers. DOI: http://dx.doi.org/10.2118/115258-MS.

[34] Tarek Ahmed, Paul D. McKinney, Advanced Reservoir Engineering. 2005: Gulf Professional. DOI: http://dx.doi.org/10.1016/B978-0-7506-7733-2.X5000-X.

[35] Crafton, James W.(1997) Oil and gas well evaluation using the reciprocal productivity index method. in SPE Production Operations Symposium. OnePetro. DOI: http://dx.doi.org/10.2118/37409-MS.

[36] Diyashev, Iskander R and Michael J Economides (2006) The dimensionless productivity index as a general approach to well evaluation, SPE Production & Operations. 21(03). 394-401. DOI: http://dx.doi.org/10.2118/94644-PA.

[37] Zeng, F and G Zhao (2007) Well testing analysis for variable permeability reservoirs, Journal of Canadian Petroleum Technology. 46(02). DOI: http://dx.doi.org/10.2118/2004-037.